Selective Laser Melting of a Bismuth Telluride Thermoelectric Materials

A. El-Desouky, A.L. Read, P. M. Bardet, M. Andre, S. LeBlanc

Department of Mechanical and Aerospace Engineering
George Washington University

Abstract

Selective Laser Melting (SLM) technology is a rapidly growing solid freeform fabrication tool because it is cost effective, reduces production time of complex shapes, and accommodates a range of material systems such as metals, ceramics, polymers, intermetallics and composites. This work presents the first-ever results for SLM performed on a semiconducting thermoelectric material, bismuth telluride (Bi_2Te_3), using a Nd:YLF pulsed laser. The evolution of the localized melt lines formed under different processing parameters such as laser power and scan speed was investigated. Melt lines were evident on the top surface of the powder compacts under all investigated processing conditions. However, cross-sections taken across the melt lines revealed material removal at the irradiation site with minimum consolidation in the subsurface. Experimental results demonstrate that it is possible to laser melt Bi_2Te_3 powder, which enables new possibilities in additive manufacturing of 3D semiconductor thermoelectric components.

Introduction

The increase of energy systems efficiency and the discovery of new sources of clean energy is a critical societal concern. More than 60% of the energy produced by power plants, cars, factories and the oil industry is lost, mostly as heat [1]. While there is continuous effort from most industries to improve energy efficiency, recovering waste heat losses is a very attractive opportunity for cleaner energy sources. Thermoelectric generators offer a potential solution for effective waste heat recovery through harvesting waste heat and converting it into useful electrical energy [2 - 4]. A thermoelectric module consists of legs of n-type and p-type semiconducting materials. These legs are connected electrically in series and thermally in parallel. The desired energy conversion is achieved through the Seebeck effect where a temperature gradient across the thermoelectric material causes electrons and holes to diffuse to the colder side resulting in a voltage drop.

A typical thermoelectric module is made of several couples, one of which is depicted in Figure 1. Figure 2 shows a schematic of traditional manufacturing steps for a thermoelectric module. First, powder materials are mixed and alloyed through high energy ball milling. The powder is then sintered in a hot pressing or spark plasma sintering die. The sintered ingots are then diced into the thermoelectric leg shapes. The dicing step on its own accounts for up to 50% of material losses due to chipping, cracking, and kerf losses [5, 6]. Furthermore, the dicing step poses geometric limitations on the thermoelectric leg shape and dimensions leading to only square or rectangular legs. Finally, module assembly costs and processing time are considerable since the thermoelectric legs are often hand-picked and placed onto the substrates.

In this paper, we propose for the first time an SLM approach as an alternative route for thermoelectric modules manufacturing. The SLM approach will eliminate the assembly of many components by enabling the production and placement of all legs into the assembly in one process while minimizing materials losses and providing geometric flexibility [7].

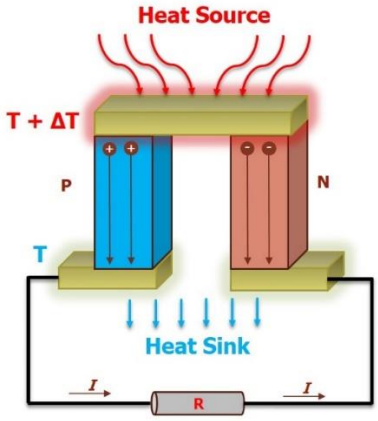

Figure 1. Schematic of a thermoelectric module in power generation mode

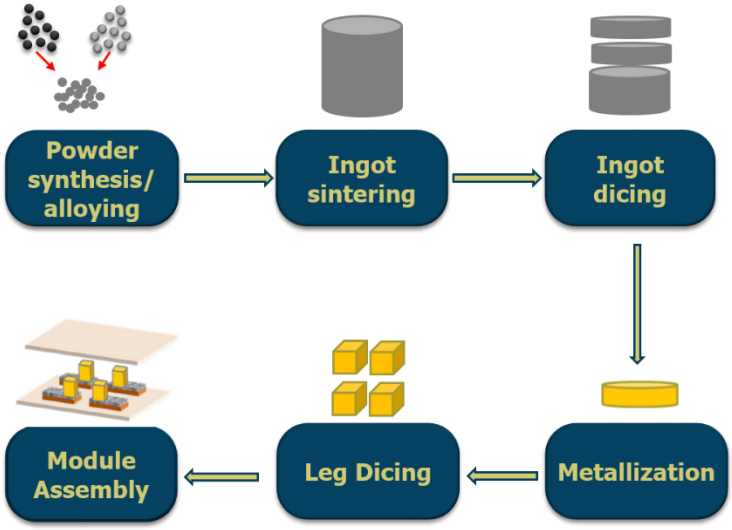

Figure 2. Traditional thermoelectric module manufacturing steps

Experiments and Methods

Bismuth telluride powder (Sigma Aldrich, −325 mesh, 99.99% trace metals basis) was used in the investigations. Figure 3 shows a scanning electron micrograph of the Bi_2Te_3. The powder lacked flowability due to its irregular morphology and agglomeration which makes it unsuitable for layer by layer deposition. The powder was instead compacted in a 7mm diameter and pressed with ~380 MPa uniaxial pressure to form 0.6 mm thick specimens.

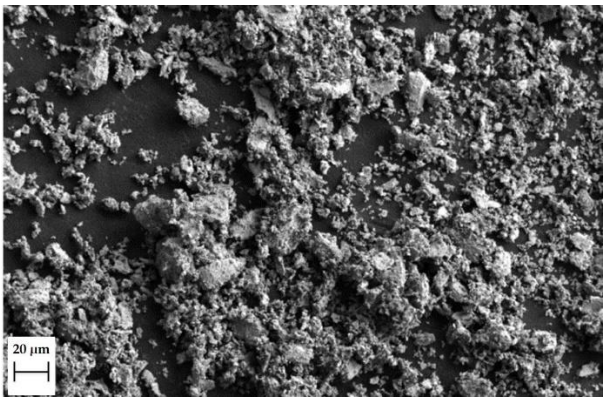

Figure 3. SEM image of Bi_2Te_3 powder.

A DM Series Dual Head High Pulse Energy (0-5 kHz) Green Nd: YLF laser (527 nm wavelength) was used to form single melt lines on the surface of the powder compacts. The laser beam was redirected from a horizontal position into a vertical position using a mirror, and it was focused to a spot size of ~173µm. Specimens were attached to an Optics Focus linear motorized translation stage (MOX-03-200) arranged in an XY configuration. The translation speed and distance were controlled using an Optics Focus Motion Controller for a NEMA17 Stepper Motor, 110V (MOC-01-1-110). Power and scan speed were varied to investigate the combined effect of laser power and exposure time on the melting of the Bi_2Te_3 powder compact surface. Figure 4 shows a schematic of the setup.

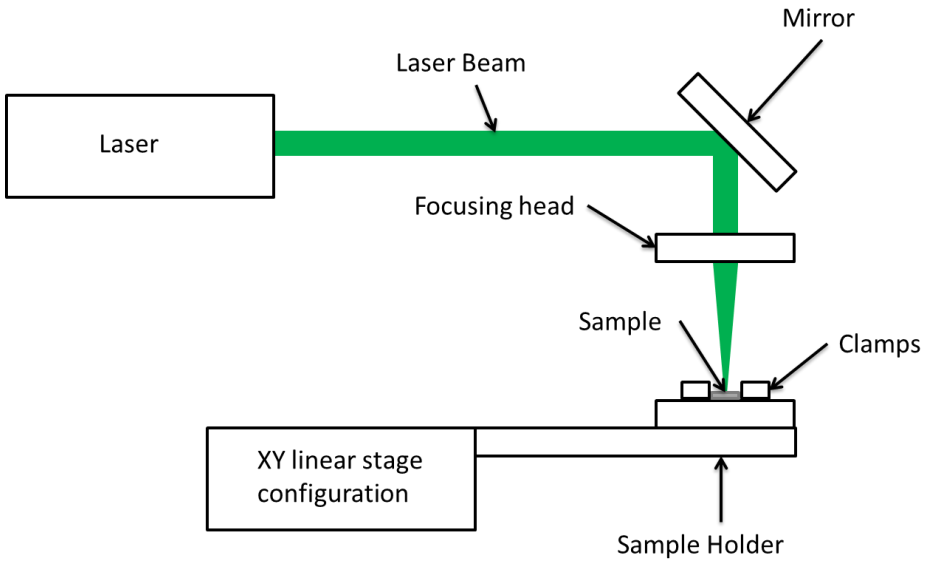

Figure 4. Schematic of the laser sintering setup.

Assuming all the input power is absorbed as heat, the average energy density E of the scan line can be calculated using the equation $E = \frac{P}{v\,D}$ where P is the average measured power, v is the scan velocity, and D is the laser spot diameter [8]. Table 1 summarizes the processing conditions

investigated in this paper. Specimens processed under a laser power of 2W and scan speed of 5 mm/s broke instantly due to the intense energy density, so they are not included in this investigation.

Table 1. Laser and scanning parameters investigated in this study. Laser power setting and scan speed combinations are indicated along with the energy density associated with each condition.

		Laser Power Input	
		1 W	2 W
Scan Speed	20 mm/s	0.29 J/mm^2	0.58 J/mm^2
	10 mm/s	0.58 J/mm^2	1.17 J/mm^2
	5 mm/s	1.17 J/mm^2	x

For microstructural observation, all specimens were cross-sectioned across the melt lines along the thickness and were ground and polished down to a 1 μm finish using liquid diamond suspension. Field emission scanning electron microscopy was conducted to examine the surface of the melt zone using a Zeiss Sigma VP.

Results and Discussion

Figure 5 shows a process zone map with scanning electron micrographs of the top surface of specimens processed under different laser power inputs and scan speeds. Distinct surface melt lines were observed in the wake of the moving laser in all specimens. It can be seen that for each laser power setting, lowering the scan speed caused material ejection which in turn resulted in deep undercuts. Using a pulsed laser with low repetition rate (5 kHz) resulted in high energy per pulse ($E_{pulse} = \frac{P}{frequency}$) which in turn led to material evaporation and plasma formation. The recoil pressure resulting from plasma formation can be advantageous as it produces a flattening effect of the melt surface. However, a combination of high energy density and high energy per pulse can result in an intense recoil pressure that will blast the powder away without sintering. Figure 6 shows a cross-section of a specimen subjected to 2W average laser power and 10 mm/s scan speed. A ~150 μm groove is visible under the point of laser incidence. The material under the groove showed no indication of melting or consolidation which suggests that material ejection was dominant rather than melting/sintering.

At an increased scan speed, the energy density is decreased, and the deep undercuts are no longer visible along the melt lines. However, the splattering around the melt line and the depression of the melt surface suggests that partial material ejection has taken place. Further investigation of the cross-sections also revealed that no melting or sintering has taken place below the top molten surface.

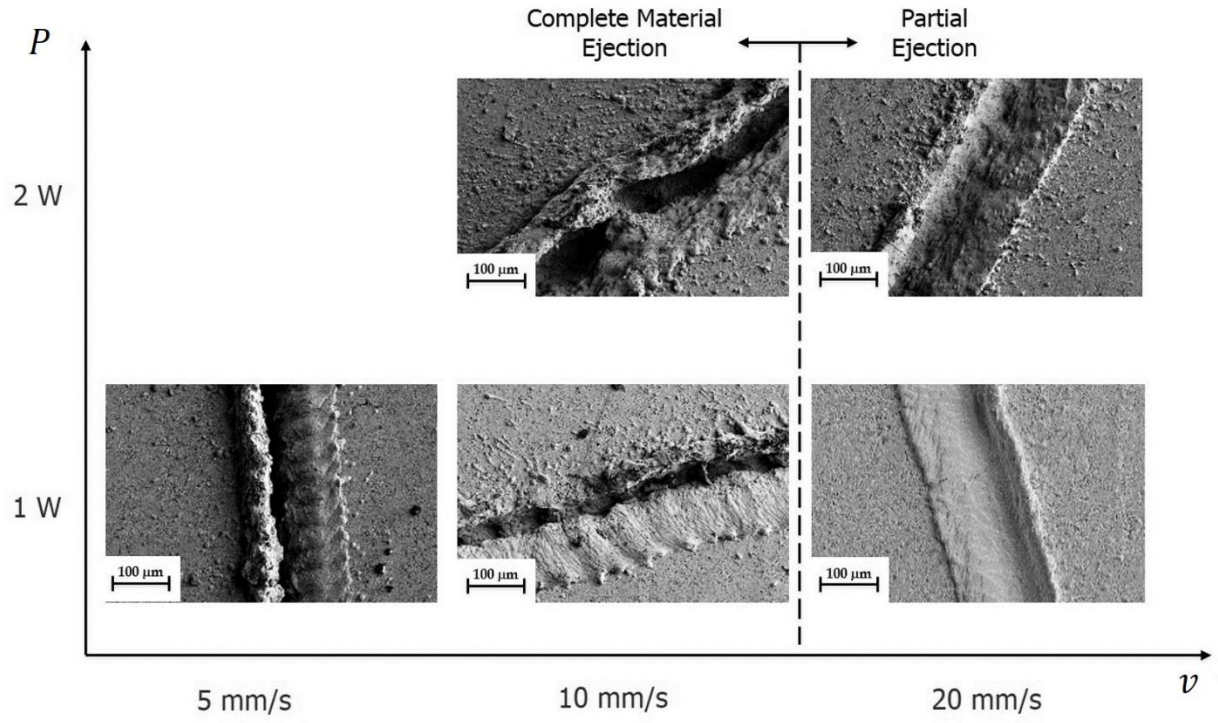

Figure 5. Process map showing SEM images of the top surface of specimens processed under different laser average power and scan speeds.

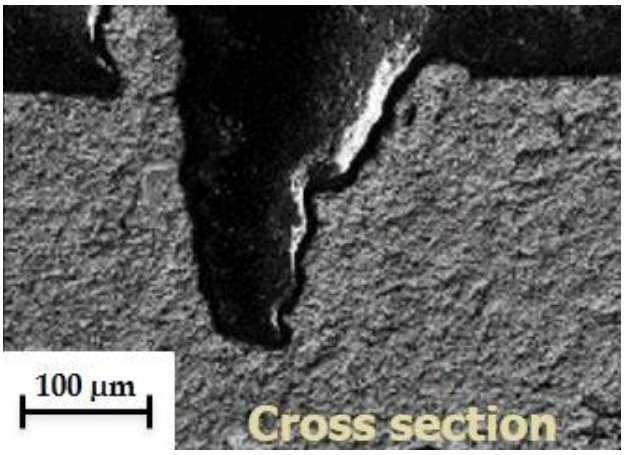

Figure 6. Cross-section view showing complete material ejection under the laser incidence for a specimen processed at 2W average power and 10 mm/s scan speed.

Typical SLM parts have a tendency to deform or crack during melting due to the thermally induced stresses that take place during material expansion and shrinkage. Materials that are ductile tend to deform, whereas materials that are brittle will crack [9]. Figure 7 shows a higher magnification SEM of the top surface of a melt line on a Bi_2Te_3 specimen processed at 1W and 20mm/s. Microcracks with random orientation are visible on the melt surface due to the brittle nature of Bi_2Te_3. Microcracks are typically avoided in SLM by preheating the powder prior to

laser processing, so a preheating step is expected to alleviate the microcracking issue observed here.

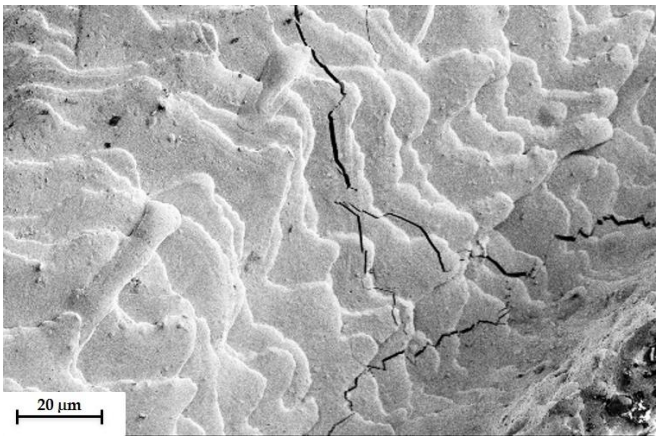

Figure 7 SEM micrograph showing microcracks on the surface of a melt line in Bi_2Te_3 powder.

Some specimens experienced a continuous asymmetrical shift in the melt pattern along the scan line due to possible misalignment of the specimen/ apparatus setup. The laser profile follows a Gaussian distribution, and, if the laser beam is not exactly perpendicular to the surface of the specimen, the slanted orientation can cause an energy density shift which will in turn result in an asymmetric melt line. Figure 8 demonstrates an exaggerated schematic of how a focal point changes when projected onto an angled surface. The energy density experienced at point 1 is half of the energy density at point 2 as the diameter of the focal point was reduced by half.

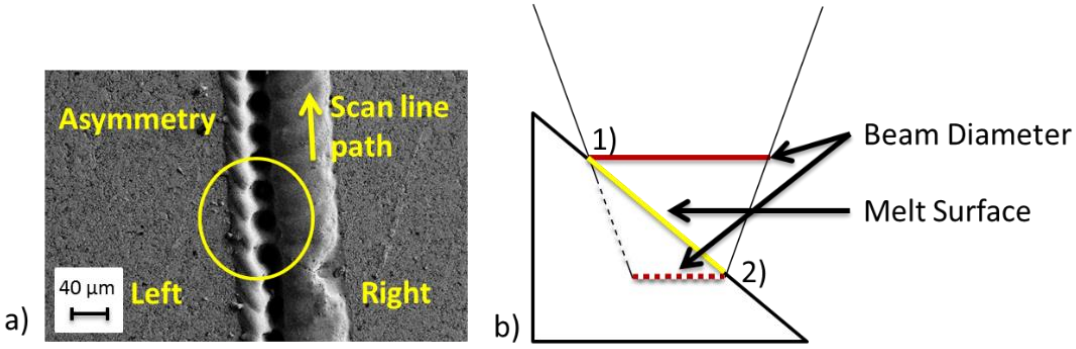

Figure 8. Example of asymmetrical melting caused by slight angling of the sample relative to the laser beam (a) and an exaggerated sketch of how the focal point changes when projected on to an angle surface (b).

At the average power and scan speed settings presented here, it was not possible to observe the evolution of the laser beam interaction with the material in a setting where material ejection is not dominant. Ongoing experiments will enable a detailed process map for Bi_2Te_3 powder processed with pulsed laser in order to find the optimum SLM parameters. In one of the more recent experiments, Bi_2Te_3 powder was processed using the same laser but with a larger spot size diameter to decrease the overall energy density and possibly avoid material ejection. Figure 9 shows SEM images of the top surface of specimen processed at 1W average power and 20 mm/s

scan speed; a flat melt line is evident with no indication of splattering or material ejection. Images at higher magnification show a solidified melt pool which was not seen in any of the results of the initial experiments.

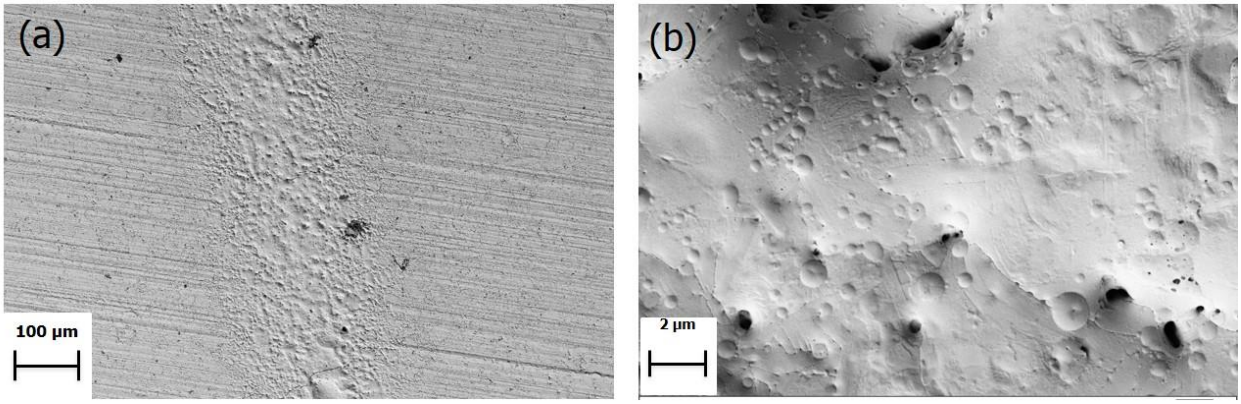

Figure 9 Scanning electron micrograph of a specimen processed using a 300 µm spot size diameter (a) and a higher magnification image taken from inside the melt line (b).

Conclusions

In the current study, SLM was utilized to melt a Bi_2Te_3 semiconductor successfully for the first time. Due to the high energy per pulse characteristics of the pulsed laser used in this study, material ejection resulting from intense plasma recoil pressure could not be avoided at a spot size setting of 175µm. However, preliminary investigations showed that complete melting of Bi_2Te_3 can be achieved at an increased spot size of 300 µm combined with low average power and high scan speed without any noticeable material ejection. While this study provides favorable proof-of-concept results for SLM of a Bi_2Te_3 semiconductor, the flowability of the powder and its ability to spread in a standard SLM layer-by-layer setup remains one of the major issues to be resolved.

References

[1] M. Martín-González, O. Caballero-Calero, P. Díaz-Chao, Nanoengineering thermoelectrics for 21st century: Energy harvesting and other trends in the field, Renew. Sustainable Energy Rev. 24 (2013) 288–305

[2] A. J. Minnich, M. S. Dresselhaus, Z. F. Ren, G. Chen, Bulk nanostructured thermoelectric materials: current research and future prospects, Energy Environ. Sci. 2 (2009) 466–479

[3] M.H. Elsheikh, D. A. Shnawah, M. F. M. Sabri, S. B. M. Said, M. H. Hassan, M. B. A. Bashir, M. Mohamad, A review on thermoelectric renewable energy: Principle parameters that affect their performance, Renew. Sustainable Energy Rev. 30 (2014) 337–355

[4] A. P. Gonçalves, C. Godart, New promising bulk thermoelectrics: intermetallics, pnictides and chalcogenides, Eur. Phys. J. B (2014) 87– 42

[5] S. LeBlanc, S. K. Yee, M. L. Scullin, K. E. Goodson, Material and manufacturing cost considerations for thermoelectrics, Renew. Sustainable Energy Rev. 32 (2014) 313–327

[6] S. LeBlanc, Thermoelectric generators: Linking material properties and systems engineering for waste heat recovery applications, Sustainable Mater. Technol. 1–2 (2014) 26–35

[7] S. LeBlanc and A. El-Desouky, Provisional Patent Application 62/164,335, 2015.

[8] J. Ciurana, L. Hernandez, J. Delgado, Energy density analysis on single tracks formed by selective laser melting with CoCrMo powder material, Int. J. Adv. Manuf. Tech. 68 (2013) 1103–1110

[9] P. Krakhmalev, I. Yadroitsev, Microstructure and properties of intermetallic composite coatings fabricated by selective laser melting of Ti-SiC powder mixtures, Intermetallics 46 (2014) 147–155